Thin fused silica shells for high-resolution and large collecting area x-ray telescopes (like Lynx/XRS)

Civitani, M., Hołyszko, J., Vecchi, G., Basso, S., Citterio, O., et al.

M. M. Civitani, J. Hołyszko, G. Vecchi, S. Basso, O. Citterio, M. Ghigo, G. Pareschi, G. Parodi, S. Incorvaia, "Thin fused silica shells for high-resolution and large collecting area x-ray telescopes (like Lynx/XRS)," Proc. SPIE 10399, Optics for EUV, X-Ray, and Gamma-Ray Astronomy VIII, 103990W (12 September 2017); doi: 10.1117/12.2275263

SPIE.

Event: SPIE Optical Engineering + Applications, 2017, San Diego, California, United States

Thin fused silica shells for a high resolution and large collecting area X-ray telescopes (like Lynx/XRS)

M. M. Civitani[a1], J. Hołyszko[a], G.Vecchi[a], S. Basso[a], O. Citterio[a], M. Ghigo[a], G. Pareschi[a], G. Toso[b], S. Incorvaia[b], G. Parodi[c]

[a]INAF-OAB, Via E. Bianchi 46, 23807 Merate (LC), Italy
[b]INAF-IASF, Via E. Bassini 15, 20133 Milano, Italy
[c]BCV Progetti, Via S. Orsola 1, 20123 Milano, Italy

ABSTRACT

The implementation of an X-ray mission with high imaging capabilities, similar to those achieved with Chandra (< 1 arc second Half Energy Width, HEW), but with a much larger throughput (2.5 m^2 effective area @1 keV), represents a compelling request by the scientific community. To this end the Lynx/XRS mission is being studied in USA, with the participation of international partners. In order to figure out the challenging technological task of the mirror fabrication, different approaches are considered, based on monolithic and segmented shells. Starting from the experience done on the glass prototypal shell realized in the past years, the direct polishing of thin (2 mm thick) fused silica monolithic shells is being investigated as a possible solution. A temporary stiffening structure is designed to support the shell during the figuring and polishing operations and to manage the handling up to its integration in the telescope structure. After the grinding and the polishing phases, in order to achieve the required surface accuracy, a final ion beam figuring correction is foreseen. In this paper, we present the technological process and the results achieved so far on a prototypal shell under development.

Keywords: X-ray telescopes, monolithic shells, fused silica, polishing, Bonnet polishing, ion beam figuring, 3M™ Trizact™

1. INTRODUCTION

The very impressive optical quality of the x-ray optics of Chandra telescope has been reached in 90s, applying grinding and polishing process to thick Zerodur glass shells. The four Wolter-I mirror shells were manufactured with a very high accuracy. As a drawback, the assembly resulted in a heavy optic with respect to the effective area of the whole telescope, which is relatively limited in spite of the large mass and volume of the optics. Nevertheless, exceptional optical performances (0.5'' HEW) have been reached [1].
In the last few years, the benefits of a similar mission concept, but with higher collecting area, started to be pointed out [2, 3, 4]. In order to fulfil the new requirements in terms of effective area (up to 2 m^2 of effective area @1 keV) keeping the costs affordable, a dedicate shell production process has been investigated by INAF/OAB [5]. The process relies on the same grinding and direct polishing approach adopted for Chandra, but with these main differences:

- The shells are made of fused silica, a cheaper material with respect to Zerodur but with adequate mechanical and thermal properties.

[1] Corresponding author: marta.civitani@brera.inaf.it

Optics for EUV, X-Ray, and Gamma-Ray Astronomy VIII, edited by Stephen L. O'Dell, Giovanni Pareschi, Proc. of SPIE Vol. 10399, 103990W · © 2017 SPIE · CCC code: 0277-786X/17/$18 · doi: 10.1117/12.2275263

- The shell thickness is reduced by a factor 10, passing from 20 mm thick shell concept of Chandra optics, to thin shells just 2 mm thick. In this way, it is possible to increase the number of the shells, and therefore the effective area, keeping limited the weight of the whole optics.
- The realization of thin fused silica shell optics is possible taking advantage of the intrinsic stiffness of the monolithic shells and adopting an ad hoc integration concept based on a Shell Supporting Structure (SSS) to be used for the handling and all the manufacturing steps [6].

The general feasibility of the direct polishing on thin glass shells was demonstrated at the end of 2012. A prototypal shell was manufactured, with a polynomial optical design and with small aspect ratio, in the framework of the Wide Field X-ray Telescope (WFXT) mission [7, 8]. Starting from a raw grinded fused silica shell produced by HERAEUS, a double cone shell was precisely grinded by LT-Ultra (Germany). A deterministic polishing process was then applied by means of IRP600 Zeeko machine based on bonnet polishing. Then, a pitch super polishing process was implemented using a dedicate pitch tool mounted on the IRP600 arm. The results of the intermediate x-ray measurement showed that the major drivers for improving the shell optical quality were the correct alignment of the optical axis of the two reflecting surfaces and the reduction of the mid-frequencies errors [9].
In order to overcome these problems and to reach the sub arc-sec requirements, the production flow of the shell has been partially revised and modified. The development of a new shell started in 2013 but the polishing of the shell wasn't completed mainly due to lack of founds [5]. The work on this shell has been restarted this year thanks to a dedicated founding program of the Italian Space Agency (ASI). This paper contains a report on the new shell manufacturing process, the tolerance analysis, the past and the recent activities on the new developed shell (called shell#4) with the last results achieved on this breadboard after the polishing process optimization.

2. PROCESS OVERVIEW

Fused Silica (SiO_2) is a synthetic molten, high purity, amorphous and non-crystalline quartz glass. It has been selected as shell substrate material for different reasons. It is relatively cheap, with a huge reduction of the costs for the entire mirror assembly (in the case of Chandra, the procurement of the shells in Zerodur was done at extremely high costs). It should be noted that the X-ray mirrors of the Einstein satellite were based on fused quartz monolithic shells. The thermo-mechanical (T/M) properties of the material (in particular low density and high Young modulus) are suitable to reach the necessary stiffness. The Coefficient of Thermal Expansion (CTE) is very low, so that it can hold up very high thermal loads. Tubes of fused silica are already available on the market. They are mainly used for the semiconductor and the solar energy applications. The Heraeus Quarzglas GmbH & Co KG normally produces tubes in fused silica with diameters up to 900 mm and wall thicknesses between 0.5 – 13 mm. Moreover, also Corning, trough the cut and grinding from the bulk material, may provide fused silica shells. In this case the realization of very large diameter shell (up to 3 m) is already in the company capabilities.

In the past years, we have already purchased several raw quartz tubes, initially with a cylindrical shape, grinded to impart a double-cone configuration, from Heraeus Quarzglas GmbH & Co KG. This is a two-steps grinding procedure. First, the external and internal surfaces of the glass tubes are both machined, by means of a row grinding process. Next, the internal surface undergoes a finer grinding operation. This second step reduces the Sub Surface Damage (SSD) depth, left by the initial row grinding. The polishing can remove the SSD of the internal surface, but the treatment with a chemical etching should be also investigated in order to address the problem for both the internal and external surfaces. The tuning of this process will be the subject of further studies. The final goal is to provide thin quartz shell with double cone profile and out of roundness in the range of 10 microns.

A Shell Support System (SSS) guarantees a 'stress free' condition and limits the deformations experienced by the shell, in particular during the machining and the calibration phases. After the development of the first shells, an additional interface to the SSS has been recently introduced in order to increase its stiffness, limiting the deformations on the shell surface, which could arise for example when the shell is dismounted from the lathe and mounted on the jig for x-ray calibration. Moreover, this sub-system, called Invar Spoke Wheel (ISW), reduces the deformations that could be introduced due to the temperature changes. The ISW is designed to follow the manufacturing process of the shell up to the final integration in the spider. It is also used to support the shell during the X-ray calibrations before the integration in the spider.

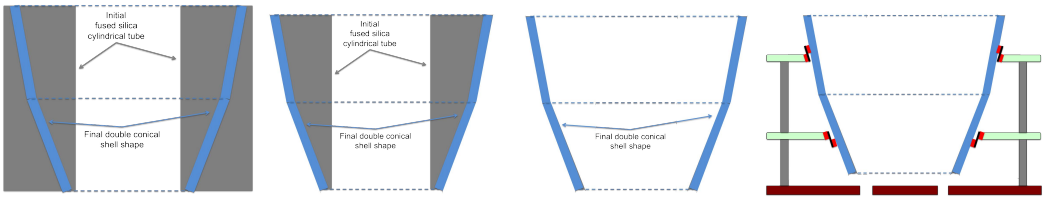

Figure 1: (A, B, C) Manufacturing process to product thin double conical shells starting from a fused silica tube. (D) Schematic drawing of the handling tool Shell Support System (SSS), to be used during the polishing operations to support the shell. Note in red the SSS/invar interface

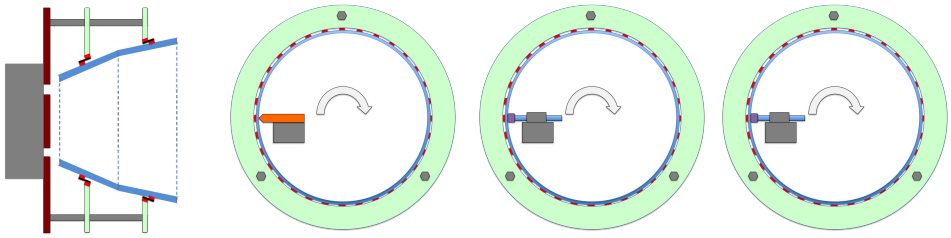

Figure 2: (A, B) Fine grinding configuration: the optical axis is horizontal and the invar interface is directly mounted on the lathe reference frame. While the shell turns, the grinding wheels machine the shell on the side. (C, D) Polishing configuration: the optical axis is horizontal and the invar interface is directly mounted on the lathe reference frame. While the shell turns, a bonnet tool before and next a pitch pad polishes a section (parabolic or hyperbolic) of the shell on the sides.

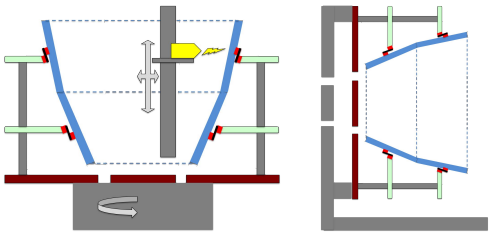

Figure 3: (A) Configuration for the Ion beam correction of the shell. The shell with the SSS and the invar interface is mounted onto a rotary table. The source will be moved along the vertical and the horizontal directions in order to follow at the correct focal distance the shell optical surface. (B) X-ray calibration configuration before the integration into the spider: the shell with the SSS and the ISW is fixed to a jig.

In the present configuration, the shell is grinded and polished in horizontal condition. It is fixed to the lathe for the entire process, preventing from the possible misalignment between the parabola and hyperbola optical axes. Therefore, the expected alignment performances are strictly related to the lathe geometrical stability.

The fine grinding operations can be performed at LT Ultra Precision Technology GmbH with grinding wheels and a metrological system that could be directly mounted on a very accurate lathe. Different optical probes, like Luphos and Lyon, are available at the LT-ULTRA laboratories. The expected correction of the azimuthal error in this phase is of the order of 1 - 1.5 microns Peak-To-Valley (PTV). From a general point of view, the impact of this error depends from the phase (in-phase or out-of-phase) of the residuals. Therefore, the degradation of the angular resolution of the shell has to be evaluated trough ray-tracing simulations assuming the acquired metrological data to define the azimuthal profiles. Target PTV values to be achieved are of the order of few hundreds of nanometres. The process is interrupted at the metrology repeatability limits. Further corrections can be realized on the shell with the final step via Ion Beam Figuring (IBF).

The polishing process can be carried out directly on the same grinding lathe. This part of the process has been partially revised with respect to the one used in 2013, with the introduction of a pre-polishing step. The pre-polishing with the Bonnet tool [10, 11] guaranties an efficient SSD removal. This DC removal does not change the profiles error but brings the micro-roughness below 10 nm RMS on the millimetre scale. Therefore, additional polishing is still necessary for the mid-frequencies errors removal. To this end, an oscillating pitch tool is mounted directly on the grinding lathe. The

process can be optimized with respect to different parameters as the kind and the grain of the abrasive, the length of the movement, the pitch tool size, its oscillation frequency and the force exerted. The target of this process is to achieve an error of about 1.3 nm RMS on spatial wavelengths between 2 mm and 10 mm. With the right settings in terms of pitch/abrasive/slurry, the same kind of oscillating pitch tool can be used for the final super-polishing of the shell, aiming at reaching a micro-roughness level below 0.5 nm RMS. At the end of the polishing activities, the accuracy on the longitudinal profiles is expected of the order of a few hundreds of nanometres PTV. This final error can be the sum of different factors, as e.g., the errors remained after the initial calibration of the stages and the thermal effects. Moreover, the floppiness of the shell makes not simple to apply the standard direct polishing approach (e.g. not based on dwell time). In any case, as long as the final micro-roughness is lower than 0.5 nm RMS, the longitudinal low frequency profile errors are theoretically corrigible with an ion beam figuring process, without degrading the micro-roughness [12]. For the present study, we intend to carry out this high accuracy figuring process on the shell by using the large ion beam facility developed in the past years at INAF/OAB. This facility, originally designed for large aspheric optics with 1.3m maximum diameters, will be up-graded in order to make possible the ion figuring of shells. The shell will be placed inside the chamber with the optical axis aligned as the gravity and a rotary table will manage the shell rotation during the ion figuring [13, 14].

X-ray calibrations of the shell can be performed at two different manufacturing stages. The first x-ray measurement can be realized after the polishing phase, to crosscheck the expected HEW with the metrological data. This calibration may be skipped if the surface quality is not adequate to reach at least 25''. The second one is foreseen once the final ion-beam figuring process, when the polishing activities on the shell are completed, with the goal to reach a sub arc second angular resolution. In order to prevent deformations in the shells, the shell still mounted into the SSS with the invar wheel interface will be installed on a jig. The invar interface and additional flexures to this jig will guarantee the necessary stiffness to the system.

3. PROTOTYPAL SHELL DEVELOPMENT

1.1 Prototypal shell configuration

The high angular resolution prototypal shells realization started as part of the feasibility study of the WFTX mission concept [8]. For that mission concept, in order to reach a total effective area of 1 m^2, three X-ray mirror modules based on around 60 shells were needed. In each module, the shell diameter was ranging between 300 mm to 960 mm. To limit the weight of the mirrors, the shell thickness were in the 2-3 mm interval. In Table 1 we report the main parameters of the shell that compose the telescope compared with the ones of a thin prototype shell realized in 2012. Moreover, they are compared with the ones of a new prototype shell that is currently under development.

Table 1: Main characteristics of the shell and of the prototypal shell#7 (realized in 2012), shell#4 (under development)

Parameter	WFXT telescope	Prototypal shell#7 (previous breadboard)	Prototypal shell#4 (new breadboard)
Focal length	5500mm	5000 mm	5000 mm
Diameter @Intersection_plane	300-960mm	487 mm	487 mm
Thickness	2-3mm	2mm	2 mm
Total length (PAR + HYP)	300mm	200mm	270 mm
Material	Fused silica	Fused Silica	Fused Silica
Mirror design	Wolter I	Polynomial	Wolter I
Weight of the shells	1.0-5.0kg	1.4kg	1.8 kg
Target HEW On axis	2'' (1'' goal)	10'' (5'' goal)	2'' (1'' goal)

In order to reach few-arcsecond angular resolution on axis (with a goal of 1''), the shells optical design changed from polynomial to traditional Wolter-I. Instead, all the other geometric parameters are maintained.

1.2 Requirements analysis

The main different errors that could contribute to the final optical performances of the shell have been discussed in a previous paper [15]. In order to allocate a budget for the shell production, an assessment on the impact of the figure errors vs frequency range has been carried out via simulations based on the Fresnel diffraction approach, to include properly the mid-frequency error domain [16]. First, the simulations were carried out on simulated roughness profiles as derived from PSD. Different PSDs with the same slope, but different normalization values, were used to generate random micro-roughness profiles. A cut-off in the PSD has been considered for wavelengths above 2 mm, as the errors on wavelength below 2 mm are the dominant ones for this energy range with this incidence angle. Reducing the amplitude of the RMS error from 2.1 nm to 1.5 nm and then further down to 0.3 nm, decreases the contribution to the HEW worsening even when the X-ray energy increases up to 7 keV.

The same approach was used for considering the profile errors. Once chosen the part of the PSD relevant to the micro-roughness with a negligible contribution in all the cases (@ 1 keV), the figure error PSD is built-up, defining the wavelength of the cut-off and the new power-law index. In this analysis, a single break in the overall PSD has been considered so that two different power laws are describing the behaviour of the optical surface depending on the frequency range. In this respect, above a certain wavelength, it could be expected that the micro-roughness is no longer the only error affecting the plates and an increase of the PSD slope can be expected. Different indexes are considered for PSD profile (1.5, 1.8, 2.8 and 3.8) and different cut-off positions (2 mm and 1 mm).

An example of the input in terms of PSD and the corresponding simulated profile containing both micro-roughness and profile errors is reported in Figure 4. The HEW is evaluated at 0.27 keV, hence the errors with spatial wavelengths below 23 µm are expected to be irrelevant and are not considered. For each of the considered PSD, ten different profiles are reconstructed from inverse FFT (Fast Fourtier Tranform) with different random phases, so that the different profiles have all the same PSD. Small differences are expected in the PTV of the single profiles but, by definition, they all have the same RMS in a given wavelength range. In figure 4B, the PTV and the RMS of the micro-roughness profile, the figure profile and the overall profile (the sum of the two) for each of the ten simulated profiles are shown. The profiles and the corresponding HEW determined values are reported in Figure 4C. The colour scale for the profile error map is in microns. As ten profiles are generated for each case, the mean RMS and PTV of the different configurations are shown in the top panel of Figure 5A. In the bottom panel the corresponding average HEW and its standard deviation are reported. In Figure 5B, the correlation between the RMS on the surface and the expected HEW is displayed. In all the considered cases, the RMS needs to be less than 30 nm in order to guarantee a contribution < 1''.

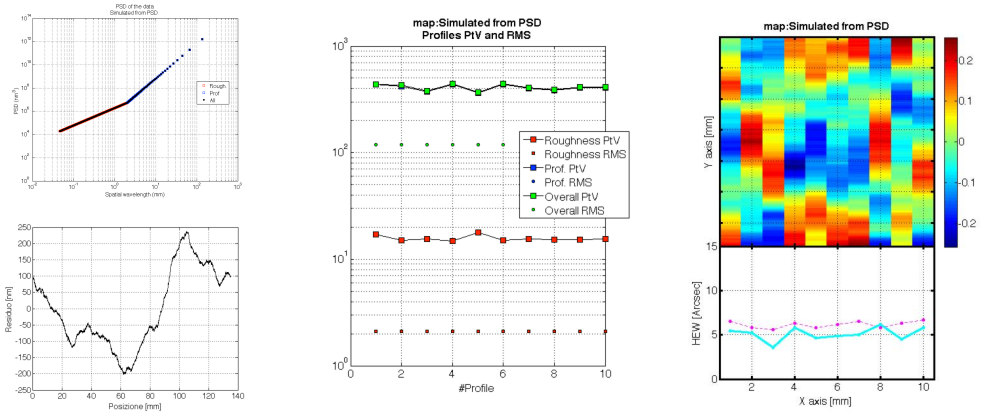

Figure 4: Left: PSD of the data generated and examples of the profiles generated for the parabolic segment of the shells. Central: PTV and RMS errors of the different profiles generated. Right: overall profiles are defined as a sum of two profiles generated independently from the two defined PSDs.

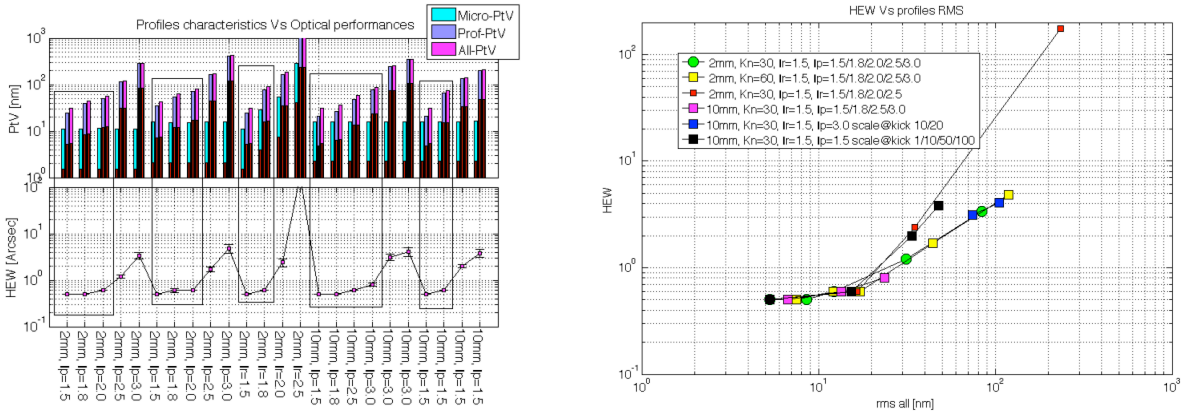

Figure 5: Overall results for the parabolic segment of the shell. HEW Vs Shell profile RMS.

1.3 Past activities performed on Shell#4 and related results: a summary

The manufacturing of the shell#4 started in 2013 but was not completed due to founding lack. In this paragraph we summarize the performed activities, reporting the final status of the shell before the activities restarting in 2017.

The initial OOR (Out Of Roundness) error of this particular shell was quite high: the initial measure, as acquired on OAB with the OOR profilometer, with the shell positioned on the astatic support (metapore made, 12 supporting points) had a maximum value @PHIMAX (the maximum diameter of the parabola) of 180 microns. The shell has been then integrated in the SSS jig (see Figure 6). During this operation, its OOR was modified of a few microns. Next, the shell has been mounted directly on the lathe using a suspension cable. The 3 spacers to interface the lathe have been directly rectified on the lathe itself. Moreover, the three contact areas on the SSS have been rectified in order not to introduce deformations in the SSS during the fixing procedure. The final centring of the shell on the lathe axis was within 10 microns with respect to the shell OOR for both parabola and the hyperbola sides. During the various phases of the shell integration (starting from the shell in free condition placed on an astatic support and ending-up with the shell integrated in SSS and mounted on LT-Ultra lathe), the errors were maintained almost constant. Instead it was evidenced a tilt of around 30° in the OOR directions once the shell is mounted on the lathe. The same phenomenon was observed during the shell integration in the SSS, when it was turned up-side/down during the installations of the flexures on the top. In that case, the tilt was observed to be about 60° in the same direction.

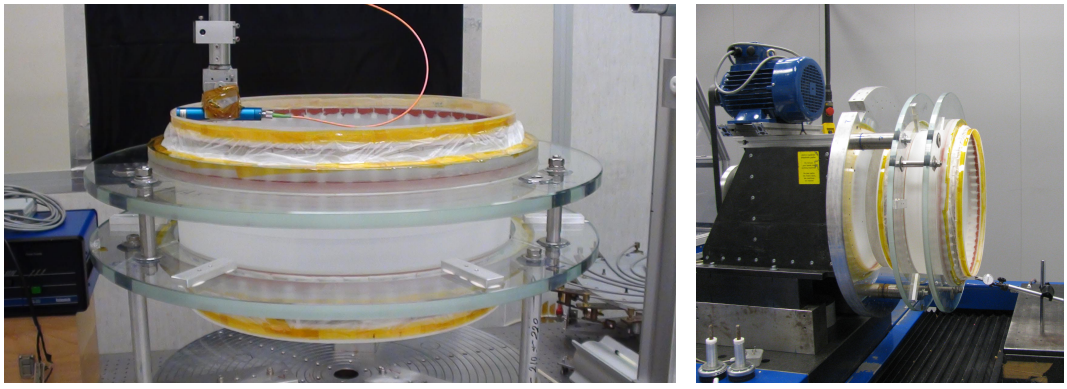

Figure 6: The shell#4 (i.e. the new breadboard) after the integration in the SSS and the fixing to the grinding lathe.

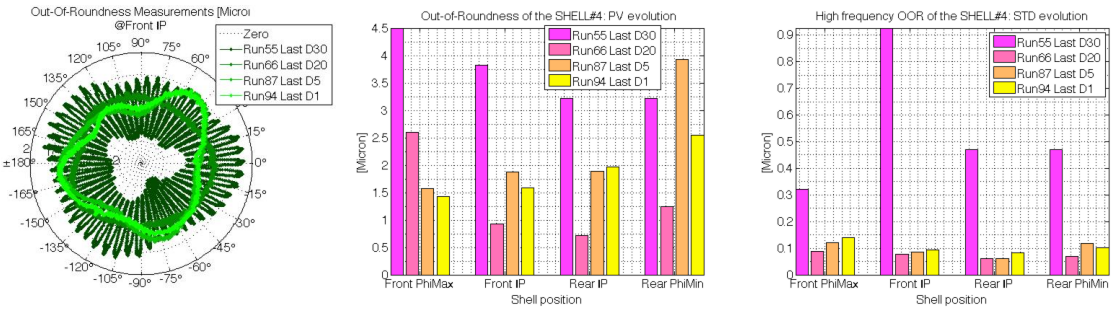

Figure 7: (A) The OOR as measured near the intersection plane on the parabolic side after the last run of the different grinding wheel (D30, D20, D5 and D1). The high amplitude azimuthal modulation is present at the end of D30 grinding runs disappears after the grinding runs with D5. (B) The PTV of the OOR @PHIMAX, @FrontIP, @RearIP and @PHIMIN for the same data set. (C) The RMS of the OOR without considering low frequency azimuthal error up to the 6th order.

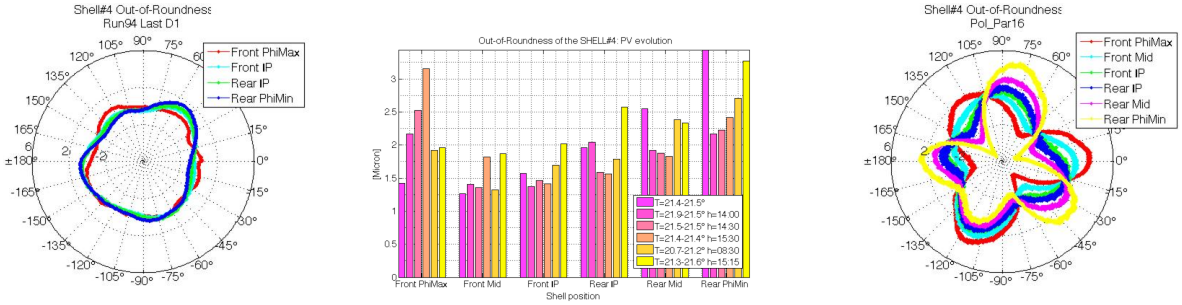

Figure 8: (A) The OOR of the overall shell @Run 94 (last run D1). (B) The outcome of the repeatability tests for the OOR measurements realized at the end of grinding phase, @run94. (C) OOR as recorded at the end of the polishing phase.

The longitudinal measures have been taken assuming a Wolter I design and a length of the shell of 135mm+135mm. These measures are acquired at the four azimuthal positions (0°, 90°, 190°, 270°). The OOR measurement positions were located at 5, 135, 145 and 265 mm from PHIMIN side (5 mm from top and bottom of Parabolic and Hyperbolic sections and from Intersection Plane (IP)).

The initial roughness measurements have been acquired on the shell at different azimuth angles (0°, 90°, 180° and 270°) and at different height levels (75mm, 125mm, 155mm and 260mm). The roughness on shell front side is higher, of around 1.3 times the roughness on rear side, and is increasing going toward PHIMAX up to 1.2 micron Rq.

The correction of the OOR was carried out with grinding wheel starting from D30 and continued with D20 and D5 and D1. The overall PTV was almost corrected with the D30, but a high frequency pattern remained on the azimuthal profile of the shell, in particular in the region of the Intersection Plane (see Figure 7A). These features, probably due to the OOR of the grinding wheel itself, were removed during the grinding with D20. In Figure 7B, the PTV of the OOR, as measured after the last run with the different grinding wheels, is shown. The best results were achieved with D20, while D5 and D1 were not effective on this aspect. In Figure 7C is reported the RMS error of the same azimuthal profile without considering the low frequency deformations (bi-lobes, tri-lobes up to the sixth degree). The value is almost constant for all the grinding wheels apart from D30. In particular, the usage of fine microstructure wheels as D5 and D1 didn't improve the error shape. The OOR correction was stopped as the repeatability of the measurement depended on the temperature in non-systematic way. The PTV of the ORR was around 1-3 microns (see Figure 8). Their impact on the HEW was of the order of 2''. The PTV and the shape of the residua changed during the polishing runs with respect to the end of the grinding phase. A clear tri-lobe appeared on PHIMAX side with a PTV of around 8 microns. A more articulated tri-lobe appeared on PHIMIN side with a PTV of around 10microns (see figure 8C). This behaviour was not fully understood. It was supposed to have been caused by a not perfect the temperature control of the environment or to the slurry that could have reached the backside of the shell (followed by the deposition or interaction with the the flexure bonding adhesive).

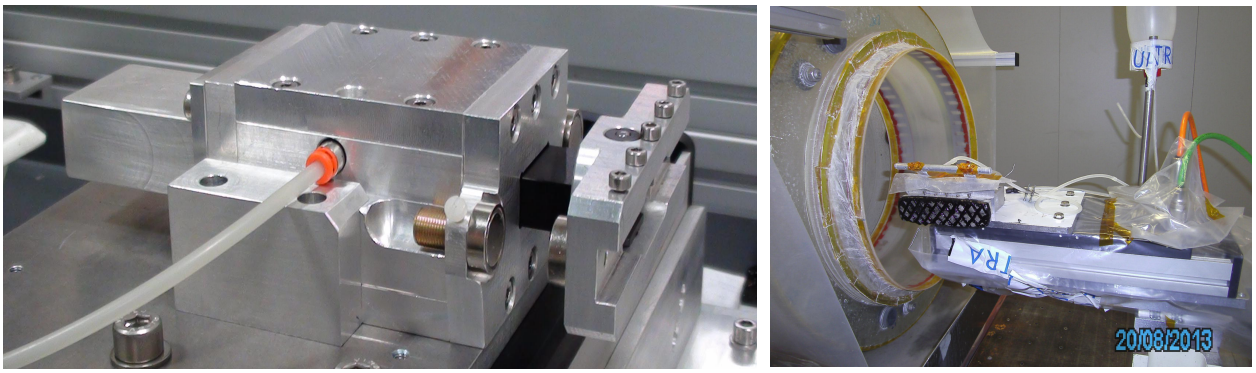

Figure 9: (A) The pitch tool support: the pitch pad is fixed to an air bearing carriage and the exercised force is fixed adjusting the distance between the magnets placed at the top and at the bottom of the pitch pad. (B) The pitch tool is driven by a linear stage mounted on the grinding lathe carriage so that it is parallel to the surface to be polished. The slurry is dispensed in drops from the top.

The grinding operations were performed with D30, D20, D5 grinding wheels. Final Rq at the end of the different phases is around 1vmicron, 0.3 micron and 0.1 micron respectively. The last grinding (with D1 wheel) has been restarted after a first polishing attempt. Final RMS was around 70 nm (Mahrr data on 5.6mm scale).

The polishing trials started in August 2013 on the grinding lathe with a dedicated polishing tool system. The pitch tool, with a contact area of 30 mm x 135 mm, is mounted on an air bearing carriage. The force exercised by the pitch tool can be adjusted by means of the set of magnets mounted in repulsive configuration. A linear carriage moves the pitch tool. It allows introducing fast oscillations up to 15 Hz on 2 mm scale. This carriage is mounted on the lathe carriage, oriented in the shell section direction and placed in position on the shell at the correct distance from the surface to get the desired force (see Figure 9).

Unfortunately, the polishing process, started on the parabolic section, did not converge in the available time. Due safety reasons the polishing was possible only during the day and even if long runs were carried out (sub-divided in several working days), this approach didn't show observable improvements. This operational constrains brought to a trial and error sequence with a final roughness a little higher than the one achieved with D1 grinding wheel. Both CeO2 slurries with 1micron and 3microns grain size were used. The micro-roughness as measured with the Mahrr is reported in figure 10 both in terms of Rq and Rz, while MFT 10x images acquired on the millimetre scale in the shell final status, are reported in figure 11. The images have been taken in 8 different azimuthal positions in three different regions of the shell: in the middle of the hyperbolic section, on the parabolic section near the intersection plane and in the middle of the parabolic section. As no polishing was operated on the hyperbola, the data acquired on this side are representative of the status of the shell after the grinding. The RMS is 45 ± 6.2 nm while the PTV is 336.2 ± 47.9 nm. The polishing on the parabola resulted in a surface roughening: near the intersection plane the RMS was 78.5 ± 11.7 nm with PTV equal to 814.6 ± 251.6 nm, while in the central region the final RMS was 54.3 ± 5.0 nm with a PTV equal to 410.2 ± 60.7 nm.

On the other side, the longitudinal profiles were unchanged by the polishing process, while the OOR started to degrade (the final PTV was of around 10 microns). The final OOR is reported in Figure 8C. Its shape does not appear easily correlated with the fixation points or with the initial one. This behaviour was not clear but as the longitudinal profiles were unchanged it appeared to be related to the shell/SSS thermal behaviour or to the interaction between the slurry and the bonding fixation junctures on the shell and of the SSS itself. The contribution of the OOR to HEW increases from around 2'' up to around 5'', with the OOR PTV passing from around 2 micron to 10 microns. The contribution of the longitudinal residual profiles on the parabolic segment is different excluding the first 5 mm or 10 mm on the parabolic segments side. Assuming a cut of 10 mm per side, the HEW is around 20'' (low frequency errors) and increases to 30'' if the cut parts are reduced to 5 mm.

At this point the polishing activity was interrupted in order to characterize and optimize the process on samples @OAB. The shell was dismounted from the lathe but remained in LT-Ultra in a box.

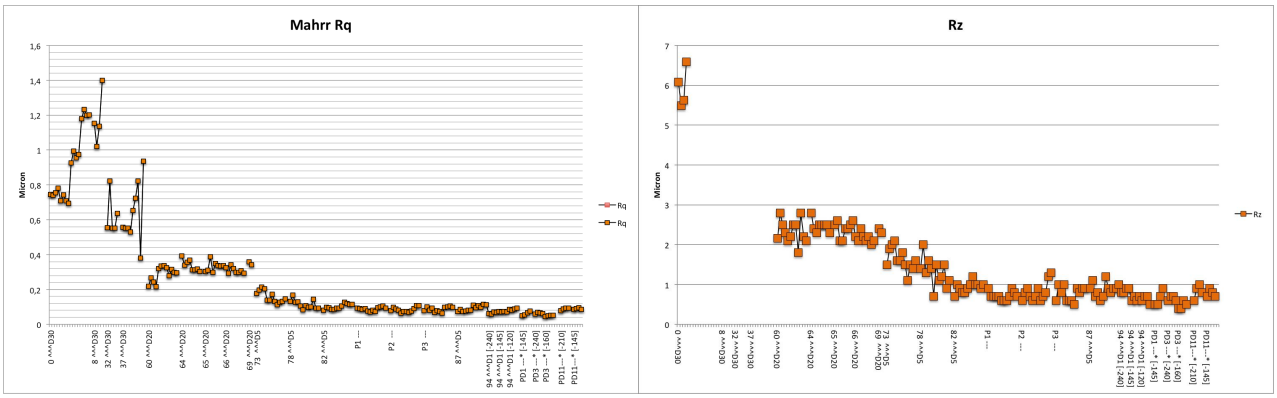

Figure 10: Micro-roughness data (Rq and Rz) acquired with the Mahrr contact instrument during the grinding and the first polishing attempts.

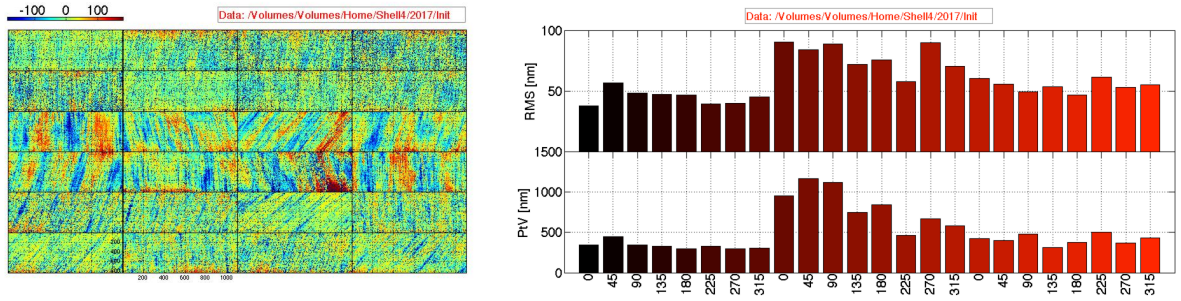

Figure 11: (A) Images acquired with MFT 10x (1mm scale) each 45° along the azimuth in different shell regions: on the hyperbolic section (grinding with D1), on the parabolic section near and in the middle region (polishing with pitch and CeO2). (B) RMS and PTV derived from the data.

1.4 Process up-grades and last results

The activities to finalize the production on Shell #4 restarted in 2016. The original SSS was composed of two rings made of Borofloat glass, hosting three couples of metallic inserts (120° spaced in azimuth). One insert of each couple is used to connect the two glass rings through metallic bars; the other inserts are used for interfaces the SSS to the lathe or to the jigs. The shell is connected to the two glass rings through a metallic thin "comb", realizing a radial flexure at the connection between the mirror shells and SSS.

In the past activities, a solid aluminium disc (60 mm thick) was used as interface to the grinding lathe. Since the environmental temperature during grinding and polishing activities could be subject to a few degrees variations, it has been substitute the Al disc by the IWS (Invar Wheel Spoke), with the end to reduce the risk of thermal distortions in the system. Moreover, this interface is supposed to remain as part of the SSS during the following activities on the Mirror Shell (MS), in order to prevent deformations on the shell induced during the different fixation phases. The entire scheme of the shell + SSS + ISW is reported in Figure 12A.

The solid Al disc had some advantages vs. the ISW in terms of stiffness (under the same mass and operational constrains). The ISW final design has been optimized to maximize the frequencies related to global modes. The lowest frequency at 127Hz (to be compared with the 152Hz of the Al disc) corresponds to an in phase tri-lobes shape (see figure 12B). During all manufacturing phases any dynamic actions operating near to this frequency (or higher frequencies) must be avoided.

In this condition the expected deformations on the shell under lateral gravity are reported in figure 12C. The contribution to the HEW is below 0.2''. When the gravity is directed parallel to the optical axis (from PhiMax to PhiMin) and the

ISW is simply supported in correspondence to location of the 8 screws, no shear forces are transmitted at screw locations and the deformations on the shell are out-of-phase tri-lobes with lower amplitude (from PhiMin to PhiMax are 2.3 microns, 0.5 microns and 2.1 microns).

The temperature deformations, at least for temperature gradients with 1°C amplitude, are always small (below 1micron) for all the different cases considered in the analysis (uniform difference in temperature between the MS and SSS+ISW, between the lathe and the MS+SSS+ISW system, gradients along the upper and the lower glass discs of the SSS etc.), with an impact in terms of HEW lower than 0.2''.

On the other side, given that the ISW is much stiffer than the SSS, the analysis of the tolerances in the contact area planarity and relative alignment, demonstrated that much care should be posed during the different fixing process and that a dedicated jig with flexures should be interfaced to the ISW when the system has to be dismounted from the lathe and e.g. adapted to perform an X-ray measurement.

The ISW was realized and mounted on the lathe just before restarting the activities with the lathe on the shell#4 in June 2017. The three spacers were fixed to the ISW and their outer surface flattened directly on the lathe (see Figure 15A). Next, the MS with the SSS was fixed to the spacers (see Figure 15B). The OOR of the shell changed of some microns, a few microns due to the centring error and a few microns due to the shape error itself. Moreover, a box with a dedicated temperature control (0.2° in stationary phase) was installed around the lathe in order to keep all the system at a controlled temperature.

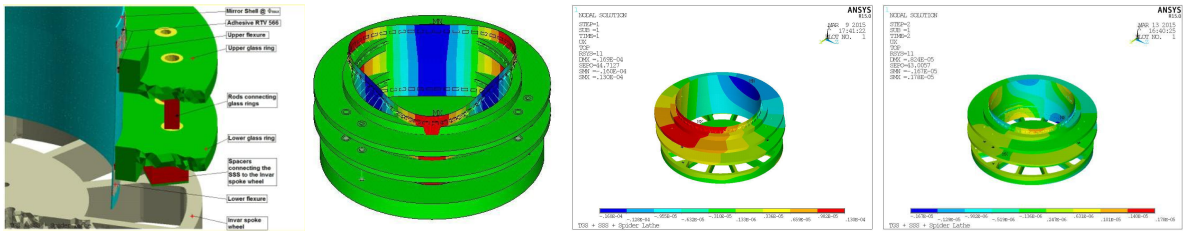

Figure 12: (A) Overview of the mechanical set-up of the Mirror Shell (MS), the shell Support System (SSS) and the Invar Spoke Wheel (ISW). (B) The OOR of the MS related to the lowest MS frequencies. The isocontours of the radial displacement component of the whole assembly under lateral gravity (C) and under axial gravity (D)

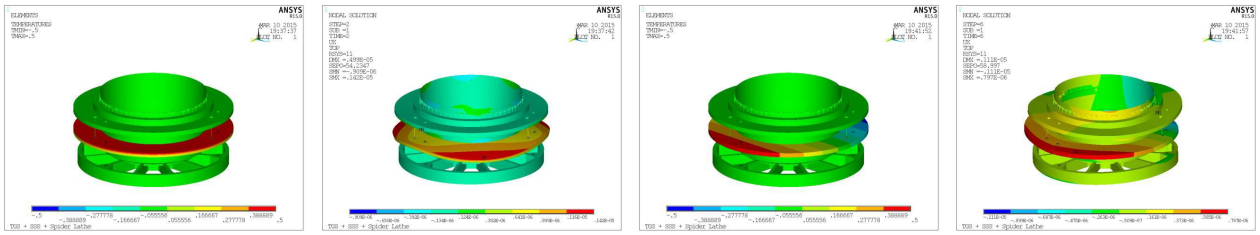

Figure 13: Examples of temperature gradients effects on the ISW + SSS + MS system. (A) A temperature gradient (1°C along the total ring thickness), in axial direction, is considered on the lower glass rings. (B) Radial displacement isocontours of the MS. (C) A temperature gradient of 1°C, in lateral direction, is considered on the lower glass rings. (D) Deformed shape with radial displacement isocontours quoted in meters.

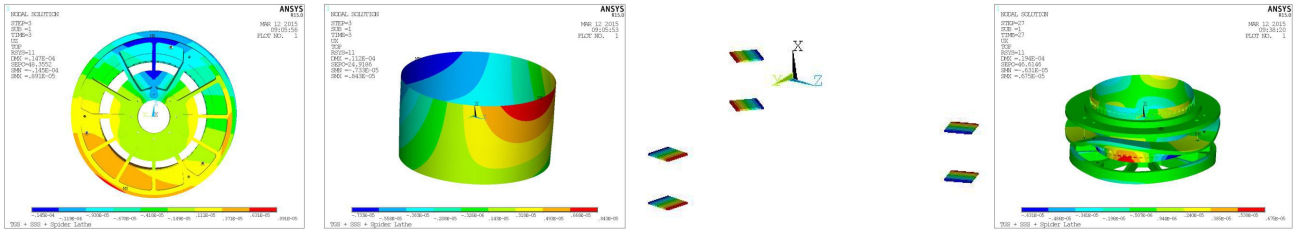

Figure 14: Example of tolerances interfaces analysis between the ISW and the lathe and between the ISW and the SSS. (A)

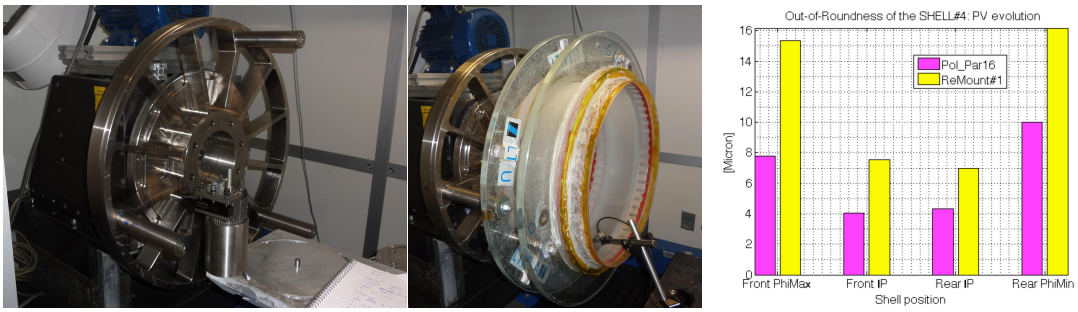

Figure 15: The ISW mounted on the lathe with the three spacers to the SSS ready to be machined. (B) The SSS with the MS is fixed to the ISW and measured in terms of OOR. (C) The PTV of the OOR in the four different shell positions as recorded during last run in 2013 and after the fixation to the ISW.

Due to the new set-up, all the activities on the shell have been to be restarted from the grinding. As the OOR to be corrected was not that high, it has been decided to operate starting from the D20 grinding wheel, which guarantees an acceptable removal rate without degrading too much the micro-roughness. Moreover, this choice avoided the generation of the azimuthal pattern emerged during the previous grinding campaign, clearly due to the D30 grinding wheel. The results previously achieved for testing on a flat fused silica sample with an ordered sequence of different grinding wheels (D30, D20, D5, D3 and D1) are reported in Table 3. For the D20 grinding wheel, the expected micro-roughness is around 300 nm RMS with PTV error of the order of 2 microns. On the contrary, the usage of all the other (D5, D3 and D1) brings the micro-roughness around 80 nm RMS with PTV of the order of 600nm.

The old data sets acquired on the shell#7 (machined at Zeeko Ltd) show that the Sub Surface Damage (SSD) left by the D30 grinding wheel was easily removed in effective way by means of an uniform removal of some microns realized in a limited amount of time (around 80 hours per semi-shell). The final micro-roughness was of the order of few nanometres RMS with a PTV error of around 20 nm. On the other hand, the tests performed on grinded samples evidence that, at even at the end of the sequence down to the D1 grinding wheel, a few microns of material had to be removed in order to get an equivalent result.

As the removal rates of the finer grinding wheels are quite low and as the PTV of the remaining features on the surface are not that small, the grinding sequence was stopped at the D20 and the bonnet polishing introduced. As the metrology on the grinding lathe is relatively simple, a bonnet polishing has been applied directly on the lathe in order to reduce the SSD. So, instead of dismounting the shell from the lathe, transporting it in OAB and using the Zeeko IRP1200 machine, the lathe configuration has been modified. A dedicated mixing device at controlled temperature was purchased for the slurry distribution. For cost limitation, this system was not equipped with the control on the slurry density (which is instead is available on the Zeeko IRP1200 machine). A mechanical interface has been prepared for the fixation of the Bonnet tools on the spindle (instead of the grinding wheels).

Table 2: Surface micro-roughness in correspondence of the different grinding wheel as measured with the Mahrr instrument (on 5.6 mm scale) and NewView instrument on 300micron scale.

Grinding wheel	**Mahrr Radial 5.6mm scale**		**Mahrr Tangential 5.6mm scale**		**NewView 0.35 x 0.26mm**		**Removal rate mm^3/min**
	Rq	Rz	Rq	Rz	Rq	Rz	
D30	0,760	4,370	0,527	3,001	933.0	6518.5	Not Available
D20	0,319	2,055	0,280	1,820	357.0	4231.1	17.3
D5	0,164	1,065	0,131	0,885	190.4	2559.8	3.5
D3	0,136	1,330	0,128	0,940	154.4	2004.8	1.1
D1	0,081	0,653	0,087	0,620	133.5	2253.1	0.5 upper limit

The standard Bonnet tools are inflated, kept at constant pressure during the polishing and oriented to the right precession angle by the Zeeko software. Clearly, this configuration was not possible on the lathe and rubber filled Bonnets have been purchased, while the precession angle fixed manually. The results of the tests operated on the Zeeko IRP 1200 @OAB show that better results are expected both in terms of removal rate and surface micro-roughness with the Inflated Bonnet. In particular, the removal rate of Filled Bonnet is around 40% less than the Inflated Bonnet. Therefore, as on the shell#7 were removed around 5microns of material (in correspondence of D30 finishing level) in about 80 hours by means of an R40 inflated Bonnet, on this shell#4 an equivalent polishing time was expected for removing around 2microns of material (in accordance with the D20 finishing level). For safety reason it was not possible to manage polishing runs lasting during the night and the process was divided into steps. In addition, in order to avoid problems in the intersection plane region, the activity was divided for parabola and hyperbola section into two different phases. The activities started from parabolic section.

In Figure 16A it is reported the Bonnet polishing configuration for the shell with the bonnet tool mounted directly on the spindle of the lathe. The micro-roughness was monitored during the process and the results, reported in Figure 16B, are relevant to the parabolic section. The Bonnet polishing activity was stopped after 78 hours of operations, as the improvement was no more effective. After around 40 hours the slope of the curve started to decrease. The Bonnet tool was exchanged with a new one, as the re-dressing operations was not possible on the lathe. This operation did not solve the problem: it was probably related to the slurry density measured well outside the standard range at the end of the process with the Zeeko IRP1200 equipment. In figure 16C is reported the dependence of the removal rate with respect to the slurry density as resulted during dedicated test carried out in OAB. The reference density value is 1.012 g/cm^3.

Unfortunately, during the metrological phase until the last run of bonnet polishing, the shell was broken due to a wrong carriage movement. The breakage passes through the shell height completely and the OOR of the shell resulted to be very much worse. On the other hand, the longitudinal profiles remained almost unchanged. An UV curing adhesive (Panacol Vitralit 6128) for Fused Silica was used to fix the shell and to allow at least a limited test of the next polishing phases.

After the bonnet polishing, the next phase should have been dedicated to the mid-frequency removal and to the micro-roughness reduction trough the high frequency movement of a pitch tool along the shell optical axis. The lapping tool was realized with a layer of pitch (pre-shaped in conical configuration) with a layer of abrasive fixed with bi-adhesive (Figure 17B). A final shaping step has to be realized on the surface to polish, heating up a little bit both the substrate and the tool. The diagonal strip pattern, with 1cm height, has been selected in order to prevent mid-frequency appearance on the tool during this operation. In principle, working all along the shell, the effect of this pattern should have been smoothed down.

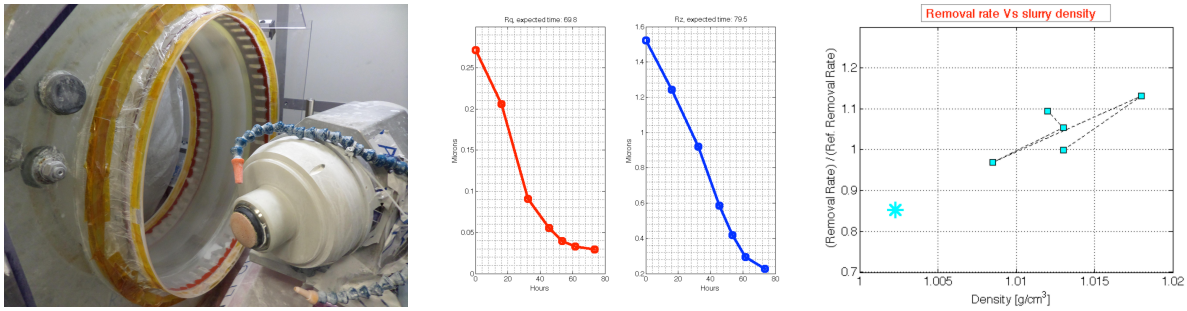

Figure 16: (A) the shell on the lathe with the Bonnet tool mounted on the spindle of the lathe. (B) The micro-roughness evolution as measured during the bonnet polishing (Rq and Rz). (C) The dependence of the removal rate with respect to the CeO2 slurry density. The point indicated with a star corresponds to the measured value of the slurry at the end of the polishing phase. The squares correspond to test results operated on the Zeeko IRP1200 machine @OAB where the slurry density can be controlled.

Figure 17: (A) The pitch tool operating on a section of the shell#4. (B) The tool structure with the 3M™ Trizact™ 568XA fixed on the pitch. (C) The 3M™ Trizact™ 568XA pyramids size evolution during the time.

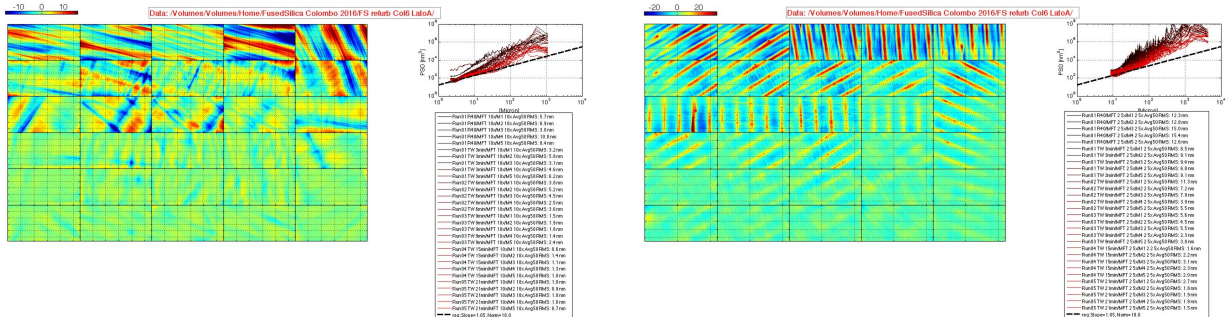

Figure 18: Flat fused silica sample figured with Filled Bonnet R40 (first line) and then polished with the pitch tool with Trizact overlayer (after 3, 6, 9, 12 and 18 minutes). Measurements are taken in 5 different positions. (A) MFT 10x results. (B) MFT 2.5x results.

The 3M™ Trizact™ abrasives feature an engineered surface of patterned, microscopic three-dimensional structures resembling pyramids. As the abrasive is used, the tops of the pyramids wear away, continually exposing fresh abrasive. As an example, in Figure 17C is reported an images of the pyramids top face at the beginning and after 258min of polishing. The advantages of this fixed abrasive for our process are the high removal rate and the low SSS in comparison with standard polishing technique. Moreover, as demineralized water is used instead of slurry, there is a huge gain in process cleanliness. Different kind of 3M™ Trizact™ abrasives has been tested, compatible with the starting condition of the shell. In particular, the results reported in the following were achieved with 3M™ Trizact™ Film Disc Rolls 568XA (white).

This polishing technique gave nice results both in terms of duration and surface quality in the test activity carried out on flats samples of fused silica. The process was tested on flat samples with starting quality similar to the shell#4 (around 70 nm RMS and around 1 micron PTV), on samples where the standard grinding down to D1 wheel was realized and on samples where a bonnet pre-polishing has been realized by means of the Zeeko IRP1200 machine at INAF/OAB. In Figure 17A and 17B the results of this last procedure, as applied on flat samples, are reported. The final RMS is around 1.96 ± 0.44 nm RMS for the MFT 2.5x (4mm scale) and 0.92 ± 0.13 nm RMS for he MFT 10x (1mm scale) after just 21 minutes staring from 13.62 ± 1.46 nm RMS and 7.12 ± 2.65 nm RMS respectively (achieved with the bonnet pre-polishing). The features left by the Bonnet tool clearly visible in the MFT 2.5x maps are progressively removed. Scaling these results to the shell, the expected polishing time was reduced to 8 hours. With a correct adjustment of the relative movements of the pitch tool with respect to the sample it was possible to manage the mid-frequencies removal. These results correspond to the pink data set of Figure 19A. These results, based on bonnet pre-polishing, are compared to the others acquired during polishing tests on flat samples in different configuration. All the data have been acquired on the millimetre scale (MFT10x data) in five different reference positions of the sample during different steps of the polishing time. The three red curves are related to the 3M™ Trizact™ 568XA polishing of sample surfaces with the initial RMS of around 70nm RMS. The reduction of the peak to valley of the surface is quite slow, of the order to tens of hours while the RMS decreases to less than 2 nm RMS in more than 15 hours. The data acquired during the polishing of a grinded are with D3 and D1wheel are reported in green. In this condition, there is a huge improvement in the process performances, probably related to the starting quality of the surface. Nevertheless, the temporal scale does not consider

the grinding time and the peak to valley error is far away from the target values with an expected converging time of more than 15 hours for D1 case.

The best results are achieved on the surface where the Bonnet pre-polishing was operated. In this case the convergence of the process is almost immediate both in terms of RMS and PTV. Furthermore the pre-polishing activity was just a matter of few hours. These results are quite promising as soon as they are scaled to the shell size. In any case, if necessary, a final step of standard pitch polishing (with loose instead of fixed abrasive) can be foreseen.

Due to the shell fracture, it was not possible to operate on all the shell, as the pitch tool could be damaged passing above the fracture. As a consequence and due to the limited amount of time remained, only two simple tests have been done. The process has been tested in the first case on an azimuthal shell section (S1) of around 12cm with the azimuthal movement realized manually (see Figure 17A). Moreover, in the second case, the polishing has been carried out on a small section (S2) with the shell fixed.

In the first azimuthal section (S1), the process was operated in steps of 6 minutes and monitoring the micro-roughness. The pitch tool frequency was set to be 15Hz, with amplitude of 2 mm. The achieved results are compared to the expected ones in Figure 19A. The data set relevant to the shell is reported in blue colour. The process performance was a little worst than expected but, due to the very 'delicate' polishing configuration, should be considered very promising. Starting from a surface with an RMS 19.7 ± 2.9 nm and a PTV of 224.7 ± 149.8nm (top part of Figure 19B), the final RMS is 1.2 ± 0.3 with PTV equal to 10.6 ± 3.5 nm (Bottom part of Figure 19B). Moreover, residual the print-through of the 3M^{TM} Trizact^{TM} 568XA pattern is related to the difficulties in the 'manual' lifting-off the tool from the surface in this preliminary raw configuration. Due to the not-optimized pitch tool configuration and to the manual action, no significant improvement in the mid-frequency was evidenced in this area (see Figure 20A). The residual profile with respect to the Wolter-I configuration of the hyperbolic section is reported on the left, while the data relevant to the parabolic one (clearly smoothed by the bonnet polishing) are reported on the right.

In the second azimuthal segment (S2), the process was monitored in two steps at 30 min and 210 min. The pitch tool frequency was reduced to 15 Hz but the stroke increased to 10 mm. The target of this test was to evidence the mid-frequency removal. This procedure is effective but the results are not homogeneous all along the shell profile. Better results were achieved near the intersection plane, probably due to a better shaping of the pitch tool in this area. In this zone, the emerging step feature is related to the abrasive pattern on the polishing pad, which is not adapted for this fixed polishing configuration.

These results are promising. The proposed technique can be certainly applied for the future shells development. Moreover, the finalization of the polishing activities on an azimuthal section on the shell#4 will be the basis for the test of the next IBF phase, providing a realistic test configuration.

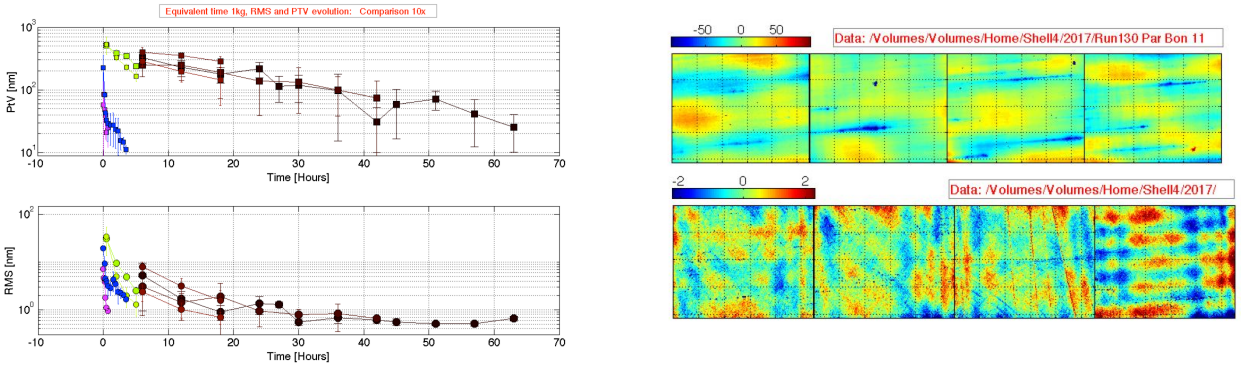

Figure 19: (A) Mean PTV and RMS (MFT 10x) as acquired in five different reference positions all along polishing steps on fused silica samples with different starting conditions (red, green and pink). In blue are reported the data of the shell#4. (B) Examples of MFT 10x maps as acquired at the end of the bonnet polishing on the shell and after the last run of polishing with 3M^{TM} Trizact^{TM} 568XA on S1 azimuthal segment of the shell#4.

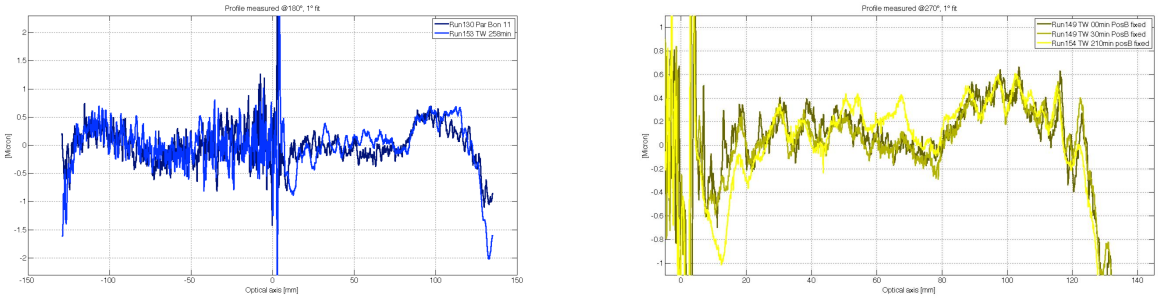

Figure 20: The residual with respect to a Wolter-I configuration of the longitudinal profiles: (A) as acquired on the S1 azimuthal section (B) as acquired on the S2 section. (At the end of the grinding, after the bonnet polishing and after the pitch polishing).

4. CONCLUSIONS

The fabrication of the mirrors for a mission that combines high resolution and large effective area (like Lynx/XRS) is a challenging task. This paper reports on the approach developed by INAF/OAB based on the direct polishing of monolithic thin (2 mm thick) fused silica shells mounted for handling in a 'stress free' condition. A temporary stiffening structure has been designed for this scope in order to support the shell during the figuring and polishing operations and to manage the handling until its integration into the telescope structure. After the grinding and the polishing phases, in order to achieve the required surface accuracy, a final ion beam figuring correction is foreseen. Starting from the experience on the prototypal shell realized in the past years, the process has been revised and upgrades have been introduced in order to guarantee better control on the results and shorter figuring time. In particular, a Bonnet polishing step was successfully introduced on a grinding lathe for the first time in order to reduce the SSD. The experimental results, achieved so far on the parabolic section of a prototypal shell under development, are very promising and the differences with respect to the expected ones is fully understood and therefore can be easily fixed. Unfortunately, due to an accident occurred during the metrological phase, the shell under development (shell#4) got broken and the figuring of the full shell is not more possible. Nevertheless, the figuring of a complete azimuthal segment will be realized in the near future, in order to test the process up to the final IBF step and a new shell is being developed based on the acquired experience.

5. ACKNOWLEDGMENTS

We thank the Italian Space Agency -ASI for its support with a contract focused on glass shell development for X-ray optics (Accordo ASI INAF 2015-041R.0 - Glass Technology for the next generation X-ray optics). We warmly acknowledge Heraeus Quarzglas GmbH & Co, LT Ultra Precision Technology GmbH KG and CAFRO Spa for the cooperation in the development of the project presented in this paper. We are grateful to Zeeko Ltd for the delivery of bonnet tools and slurry dispenser that have been mounted on the lathe for SSD removal.

6. REFERENCES

(1) M.C. Weisskopf, et al., "Chandra X-ray Observatory (CXO): overview", Proc. SPIE Vol. 4012, p. 2-16 (2000)
(2) Vikhlinin, et al., "SMART-X, "Square Meter, Arcsecond Resolution X-ray Telescope", et al., Proc. "X-ray Astronomy: the next 50 years", Mem SAIt, (2013)
(3) Weisskopf, M. C., et al., "Beyond Chandra – the X-ray Surveyor," Proc. SPIE 9510, (2015).
(4) Gaskin, J., et al., Lynx Observatory and Mission Concept Status, Proceedings of the SPIE, Volume 10397, paper 29, in press (2017, present Volume)
(5) O. Citterio, M. M. Civitani, G. Pareschi, S. Basso, S. Campana, P. Conconi, M. Ghigo, E. Mattaini, A. Moretti, G. Parodi, G. Tagliaferri, "Thin fused silica optics for a few arcsec angular resolution and large collecting area x-ray telescope," Proc. SPIE 8861, Optics for EUV, X-Ray, and Gamma-Ray Astronomy VI, 88610V (2013);

(6) L. Proserpio, et al.," Design and development of thin quartz glass WFXT polynomial mirror shells by direct polishing", Proceedings of the SPIE, Volume 7732, article id. 77320D, 14 pp. (2010).
(7) S.S. Murray, "Wide field x-ray surveys: wide field x-ray telescope (WFXT) and notional wide field imager (N-WFI)", Proceedings of the SPIE, Volume 8443, article id. 84431L, 8 pp. (2012)
(8) P. Conconi, et al., "A wide field X-ray telescope for astronomical survey purposes: from theory to practice", Monthly Notices of the Royal Astronomical Society, Volume 405, Issue 2, pp. 877-886 (2010),
(9) M. Civitani, et al., "Thin glass shell oriented to wide field x-ray telescope", Proceedings of the SPIE, Volume 8443, article id. 84430Q, 13 pp. (2012)
(10) O. Citterio, et al., "Progress on precise grinding and polishing of thin glass monolithic shell (towards WFXT)", Proceedings of the SPIE, Volume 8147, article id. 814714, 11 pp. (2011)
(11) D. D. Walker, et al., "Precessions process for efficient production of aspheric optics for large telescopes and their instrumentation", Proc. SPIE, 4451, 267 (2002)
(12) Wenin Liao, Yifan Dai, Xuhui Xie, and Lin Zhou, "Morphology evolution of fused silica surface during ion beam figuring of high-slope optical components"Appl. Opt. 52, 3719-3725 (2013)
(13) M. Ghigo, S. Cornelli, R. Canestrari, D. Garegnani, "Development of a large ion beam figuring facility for correction of optics up to 1.7 m diameter" PROC SPIE 7426, 742611 (2009).
(14) M. Ghigo, G. Vecchi, S. Basso, O. Citterio, M. Civitani, E. Mattaini, G. Pareschi, G. Sironi, "Ion figuring of large prototype mirror segments for the E-ELT", Proc. SPIE 9151, (2014)
(15) M. M. Civitani, O. Citterio, M. Ghigo, E. Mattaini, G. Pareschi, G. Parodi, "Thin monolithic glass shells for future high angular resolution and large collecting area x-ray telescope," Proc. SPIE 8884, Optifab 2013, 88841R (2013/10/15);
(16) Raimondi, L., Spiga, D., "Mirror for X-ray telescopes: Fresnel diffraction-based computation of point spread functions from metrology," AA 573, A22 (2015)